Effects of Autoionizing Resonances on Wave-Packet Dynamics Studied by Time-Resolved Photoelectron Spectroscopy

Pengju Zhang, Van-Hung Hoang, Chuncheng Wang, Tran Trung Luu, Vít Svoboda, Anh-Thu Le, and Hans Jakob Wörner

Phys. Rev. Lett. **130**, 153201 — Published 12 April 2023

DOI: 10.1103/PhysRevLett.130.153201

Effects of autoionizing resonances on wave-packet dynamics studied by time-resolved photoelectron spectroscopy

Pengju Zhang[1*,†], Van-Hung Hoang[2,3*], Chuncheng Wang[1,4],
Tran Trung Luu[1,5], Vít Svoboda[1,7], Anh-Thu Le[2,6,‡], Hans Jakob Wörner[1]
[1] *Laboratory for Physical Chemistry, ETH Zürich, Vladimir-Prelog-Weg 2, 8093 Zürich, Switzerland*
[2] *Department of Physics, Missouri University of Science and Technology, Rolla, Missouri 65409, USA*
[3] *Current address: Department of Physics, Kansas State University, Manhattan, Kansas 66506, USA*
[4] *Current address: Institute of Atomic and Molecular Physics, Jilin University, 130012 Changchun, People's Republic of China*
[5] *Department of Physics, The University of Hong Kong, Pokfulam Road, SAR Hong Kong, People's Republic of China*
[6] *Department of Physics, University of Connecticut, 196A Auditorium Road, Unit 3046, Storrs, CT 06269*
[7] *Current address: JILA, University of Colorado, Boulder and the National Institute of Standards and Technology, Boulder, Colorado 80309, United States*

(Dated: February 16, 2023)

We report a combined experimental and theoretical study on the effect of autoionizing resonances in time-resolved photoelectron spectroscopy. The coherent excitation of N_2 by ~ 14.15 eV extreme-ultraviolet (XUV) photons prepares a superposition of three dominant adjacent vibrational levels ($v' = 14 - 16$) in the valence $b'\ ^1\Sigma_u^+$ state, which are probed by the absorption of two or three near-infrared (NIR) photons (800 nm). The superposition manifests itself as coherent oscillations in the measured photoelectron spectra. A quantum-mechanical simulation confirms that two autoionizing Rydberg states converging to the excited $A\ ^2\Pi_u$ and $B\ ^2\Sigma_u^+$ N_2^+ cores are accessed by the resonant absorption of NIR photons. We show that these resonances apply different filters to the observation of the vibrational wave packet, which results in different phases and amplitudes of the oscillations depending on the nature of the autoionizing resonance. This work clarifies the importance of resonances in time-resolved photoelectron spectroscopy and particularly reveals the phase of vibrational quantum beats as a powerful observable for characterizing the properties of such resonances.

Photo-induced wavepacket dynamics is one of the central topics in femtochemistry [1] and attosecond physics [2]. A wavepacket is formed whenever a coherent superposition of several eigenstates is prepared [3–10]. The corresponding wave-packet dynamics can be effectively studied using time-resolved pump-probe spectroscopy. A particularly powerful method to probe such dynamics is time-resolved photoelectron spectroscopy (TRPES), owing to its sensitivity to both electronic and structural dynamics [11–15].

An important open question in TRPES is the role of resonances in the probe step on the observed dynamics. Such resonances are the rule rather than the exception when ionization is performed with long-wavelength, in particular visible or ultraviolet, light sources. Resonances can occur as an intermediate step in multi-photon absorption or at the final step in both single- and multi-photon absorption. Previous evidence suggests that intermediate resonances can lead to significant differences in the time-dependent signals. For example, a recent study of perylene has shown evidence of a sub-picosecond relaxation dynamics when probed through resonance-enhanced multiphoton ionization, whereas no such relaxation was visible when single-photon probing was used [16]. Similarly, a recent study of the excited-state dynamics in SO_2 using 3-photon ionization at 400 nm found pronounced vibronic wave-packet dynamics [17], whereas a single-photon TRPES study did not observe such dynamics [18]. In both perylene and SO_2, it is likely that the presence of intermediate resonances is responsible for the different time-dependent signals obtained from probing the same wave-packet dynamics.

In comparison to the case of intermediate resonances, the case of final, autoionizing resonances is even less understood. These autoionizing resonances are likely to contribute to most TRPES studies in which ionization is performed within a few electron-Volts of the threshold because of the presence of dense series of Rydberg states converging to the electronically excited states of the molecular cation. To fully characterize and understand the effect of such resonances, it is desirable to select a system with a well-known electronic structure, such that all states can be assigned and which is simple enough that the effect of different resonances can be fully resolved. Moreover, the system should support clear and long-lived wave-packet dynamics that can then be probed through different resonances, highlighting their specific roles in the TRPES probe step. Adding the knowledge gained from recent time-resolved studies of N_2 [19–25], we identified this system as a promising candidate for the present study.

In this letter, we report a combined experimental and

*These authors equally contribute to this work.

theoretical study of time-dependent wavepacket dynamics in N_2 prepared by broadband XUV (14.15±0.07 eV) excitation and probed by two or three near-infrared (NIR) photons, accessing several autoionizing resonances. The broadband XUV excitation, the short cross-correlation time and the vibrationally resolved TRPES allow us to observe (i) quantum beats between three dominant high-lying vibrational levels within the same electronic state and (ii) the dependence of the phase and amplitude of these quantum beats on the autoioinizing Rydberg states above the first ionization threshold populated by the probe laser.

The experimental setup was previously described in Ref. [26]. A fundamental NIR pulse (800 nm, 30 fs, 5 kHz) was divided by a beam splitter (70:30). The major portion ($\sim$ 0.5 mJ) was used for high-harmonic generation, providing the XUV-pump (H9) pulse. The minor portion, serving as the probe pulse, was independently focused on the gas jet in the second arm of the interferometer. The time delay between the XUV-pump and NIR-probe pulses was scanned between -130 and $+2150$ fs in steps of 10 fs. The XUV-NIR cross correlation of $\sim$ 50 fs was estimated by the laser-assisted photoelectric effect [27] of carbon dioxide ionized by a $(1+1')$ scheme. The NIR probe intensity of 2×10^{12} W/cm^2 was estimated based on the Stark shift of the photoelectron bands. The advantage of the selected pump-probe scheme is that no single-photon (XUV or NIR) ionization event is observed, thus providing a background-free scheme with only pump-probe pathways contributing to the signal.

The experimental results were simulated using the coupled-channel time-dependent Schrödinger equation for N_2 interacting with pump and probe laser pulses. Our theoretical method was reported earlier [28]. For the treatment of photoelectrons, we follow the method proposed in Refs. [29–31]. We included the N_2 ground electronic state ($X^1\Sigma_g^+$), as well as several excited electronic states based on their symmetries and energies. Specifically, we included the diabatic states b', c', and e' of $^1\Sigma_u^+$ symmetry, around 14 eV above the ground state in the Franck-Condon (FC) region [32–34], which couple strongly with the ground state by the pump pulse. Diabatic states b, c, and o of $^1\Pi_u$ symmetry, which also have energies near 14 eV were not taken into account since they play a less important role as confirmed by the experiment. Moreover, two Rydberg states, $4p\pi_u(^1\Sigma_g^+)$ converging to $A^2\Pi_u$ and $4s\sigma_g(^1\Sigma_g^+)$ [35] converging to $X^2\Sigma_g^+$, were included because they are accessed by the probe pulse. In addition, the autoionizing Rydberg states $3d\sigma_g$ ($^1\Sigma_u^+$) converging to $B^2\Sigma_u^+$, and $11d\sigma_g$ [36, 37] converging to $A^2\Pi_u$, were included as well since they couple to the intermediate b' state by a two-photon transition and are enhanced by a resonance at 17.15 eV (v= 0) and at 17.25 eV (v= 3), respectively. These autoionizing states decay to the ground electronic state of N_2^+ ($X^2\Sigma_g^+$), which is also included in the calculation.

The diagonal matrix elements of the Hamiltonian are $H_{ii} = T_R + V_{ii}$, where $T_R = -\frac{\partial^2}{2\mu\partial R^2}$ is the nuclear kinetic energy operator and $V_{ii}(R)$ is the potential energy of channel i. The dynamic ponderomotive energy $U_p(t)$ is added to the energies of the highest three channels, and the electron kinetic energy $E = k^2/2$ is added to the ionic state energy. The off-diagonal matrix elements are $H_{ij} = \vec{E}(t) \cdot \vec{d}_{ij}(R) + V_{ij}(R)$, where $\vec{d}_{ij}(R)$ is the dipole coupling between channels i and j and V_{ij} is the electronic coupling of different diabatic states. The potential energy curves (PECs) illustrated in Fig. 3 and transition dipoles are taken from Refs. [33, 38] and Refs. [33, 39], respectively. The XUV (NIR) pulse is modeled with a Gaussian envelope with the duration of 25 fs (40 fs) and photon energy of 14.15 eV (1.55 eV). The pump-probe photoelectron spectrum is calculated as

$$S(E) = \sum_i \int |\chi_i(R,E)|^2 dR, \tag{1}$$

where $\chi_i(R,E)$ is nuclear wave function, and the sum is taken over the ionic state channels.

Figure 1(b) shows the experimental two-dimensional (2D) TRPES, and the corresponding one-dimensional (1D) photoelectron spectrum integrated over all the time delays is shown in Figure 1(a). The spectrum is truncated around 0.3 eV due to the maximum acquiring limitation of the time-of-flight device. In Figure 1(b), no photoelectron signals are observed prior to time zero, and two distinct groups of photoelectron signals showing up during the cross-correlation. Peaks below 1.66 eV are assigned to the transition of one XUV plus two NIR photons, whereas peaks above 1.66 eV correspond to one XUV plus three NIR photons. An intuitive mechanism behind the observation is depicted in Fig 3. From here on, we mainly focus on the discussion of the spectra induced by two-NIR absorption.

The two-NIR-photon region is dominated by a peak around 1.55 eV assigned to a transition from the neutral ground state to the b' $^1\Sigma_u^+$ valence state (XUV pump), which is subsequently excited to the Rydberg state $3d\sigma_g$ (v$'$ = 0) [36, 37, 40] (NIR probe). This state autoionizes to the ionic ground state $X^2\Sigma_g^+$ (v$''$ = 0). Similarly, the second-strongest peak around 1.66 eV is assigned to the autoionization of the Rydberg state $11d\sigma_g$ (v$'$ = 3) [36] to $X^2\Sigma_g^+$ (v$''$ = 0). The measured energy difference of 0.11 eV between these two peaks verifies the corresponding energy gap between the respective Rydberg states. In the same way, three pairs of peaks below 1.55 eV are assigned as transitions to $X^2\Sigma_g^+$ (v$''$ = 1, 2, 3). Two extra peaks assigned as transitions from autoionization of the Rydberg state $8d\pi_g$ (v$'$ = 3) [36, 37, 41, 42] to $X^2\Sigma_g^+$ (v$''$ = 2, 3) aslo appear in this region.

The previously discussed peaks have also different time evolutions. Around time zero, all signals from different Rydberg states appear at the same time. After the

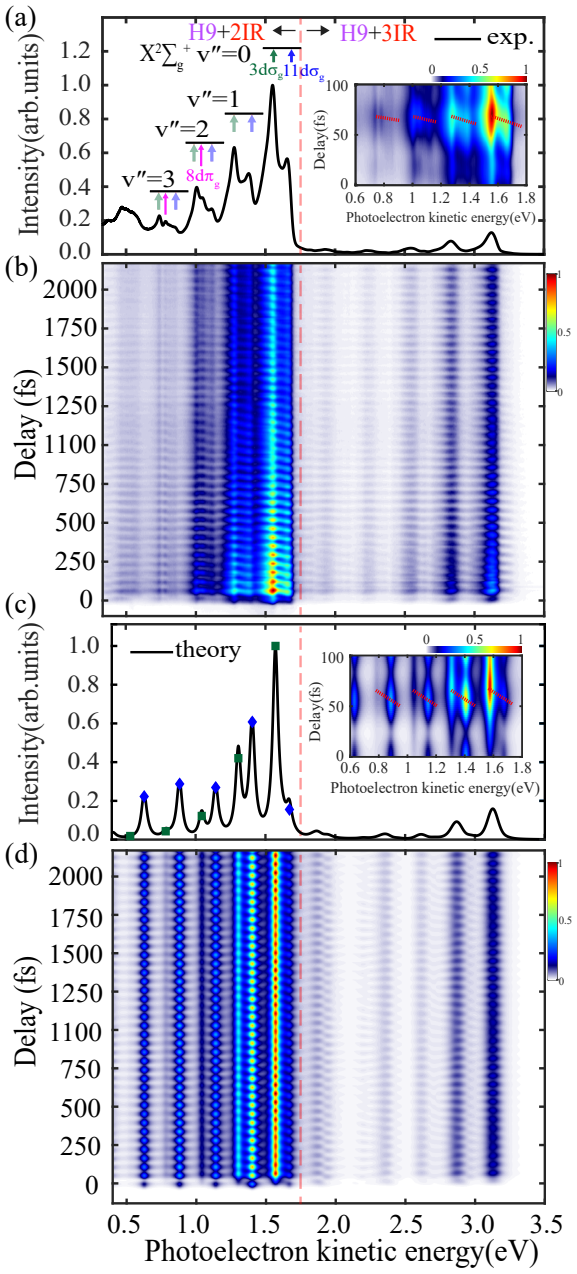

Figure 1: (Color online) (a) Integrated measured and (c) simulated photoelectron spectrum of N_2 following XUV (H9) pump excitation and NIR (800 nm) multiphoton absorption, the peak assignments for two NIR photons absorption are shown on the top. (b) Experimental and (d) simulated 2D-TRPES. The region from 0 to 100 fs shown in the insets of (a) and (c) respectively. Positive delay represents that the NIR probe pulse follows the XUV pump pulse. Simulated photoelectron spectrum is convoluted with a 40-meV Lorentzian line shape. The FC factors for sub-peaks (blue diamonds) and main-peaks (green squares) are shown in (c) respectively.

cross-correlation time, the signal from the $11d\sigma_g$ ($v' = 3$) state shows up before the one from the $3d\sigma_g$ ($v' = 0$) state (see the inset in Fig. 1(a)), and the spectrum exhibits clear beating with a period of about 50 fs. Moreover, the relative time difference between $11d\sigma_g$ ($v' = 3$) and $3d\sigma_g$ ($v' = 0$) to $X^2\Sigma_g^+$ ($v'' = 0, 1, 2, 3$) amount to 12.0±1.2 fs, 9.7±0.8 fs, 7.7±1.0 fs and 2.7±0.8 fs, respectively (see the red dashed lines in the inset and the Fig. S1 in Supplemental Material [48]). In the following, the signal originating from $3d\sigma_g$ ($v' = 0$) and $11d\sigma_g$ ($v' = 3$) is referred to as "main" and "sub" peaks, respectively.

Figure 1(c) shows the calculated photoelectron spectrum. The calculation reproduces all main features from the measured spectrum well in both the two-NIR-photons and three-NIR-photons regions. The main and sub-peaks are clearly visible in the calculation and their positions correspond to the measured peaks within 0.02 eV. However, the intensity ratio between the main and sub-peaks differs between the calculation and the experiment. This is mainly due to an incomplete evaluation of the FC factors in the theory, shown as blue diamonds (sub-peaks) and green squares (main-peaks), respectively. The calculations also underestimate the photoelectron background between in the region of 0.3-1.5 eV, which we attribute to the fact that the direct-ionization (as opposed to the autoionization) channels are not included. Figure 1(d) shows the calculated 2D spectrum which can be directly compared with Figure 1(b). The calculations predict clear beating signals for all main and sub-peaks in the two-NIR-photons region in excellent agreement with the experiment. We note that the amplitude of the calculated beating signal is constant, whereas it decays in the experiment as a consequence of rotational dynamics that are not included in the calculations.

Time-dependent profiles for main and sub-peaks are shown in Figure 2(a) and (b), respectively. All traces have similar time profiles with a well resolved beating pattern and an exponential intensity decay. The beating pattern is encoded into amplitude revivals which depend on time delay. This is due to the anharmonicity of the $b'\ ^1\Sigma_u^+$ PEC [43, 44] causing non-equidistant vibrational level spacings. Therefore, the initially well-localized wavepacket dephases over time. The exponential intensity decay is characterized with a single time constant of ~ 8 ps, which is in good agreement with an expected value derived from the known rotational constant of the $b'\ ^1\Sigma_u^+$ state [42, 45], and the assumption that the XUV excitation prepares a certain degree of rotational coherence, which later undergoes dephasing and overall decrease of the measured beating signal.

Figure 2(c) and (d) show Fourier analysis of both experimental and theoretical 2D spectra, respectively, providing further insights into the nuclear dynamics. The main-peaks have two dominant frequencies: one around 17.5 THz corresponding to beating between b' ($v' = 15$) and ($v' = 16$) states and the other around 18.8 THz corresponding to beating between b' ($v' = 14$) and ($v' = 15$) states, shown as inset in Fig. 2(a). Identification of these two beating frequencies confirms our assignment that three adjacent vibronic levels are simultaneously prepared by the XUV pulse. Referring to the inset in Fig. 2(b), for the sub-peaks, only one dominant frequency around 17.5 THz is observed, which is explained below.

As discussed above, the sub-peaks appear earlier than

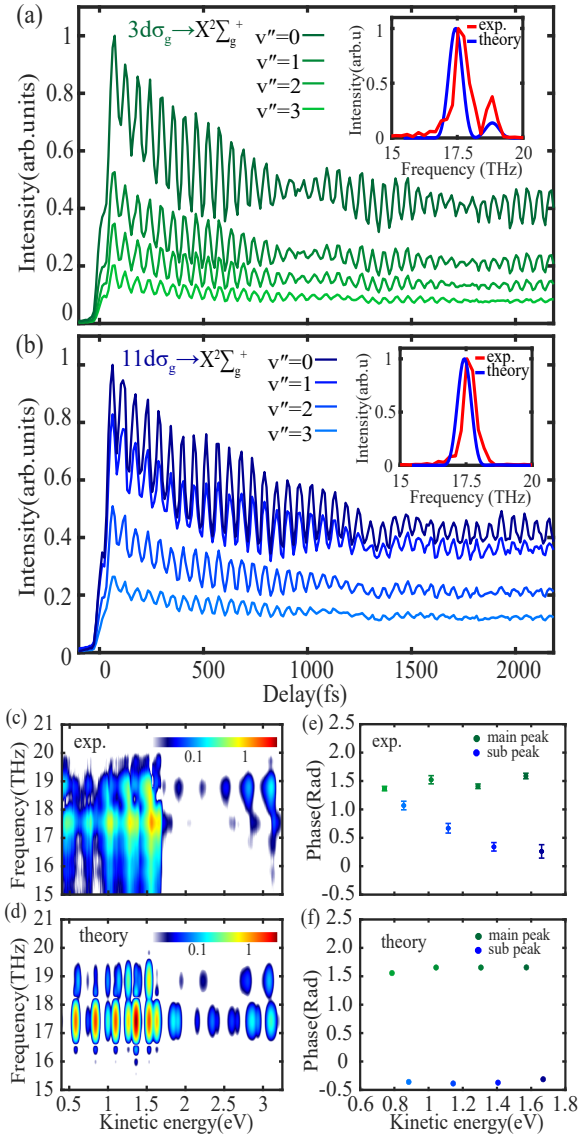

Figure 2: (Color online) (a) and (b) The integrated spectra of the transitions from $3d\sigma_g$ ($v' = 0$) and $11d\sigma_g$ ($v' = 3$) to $X^2\Sigma_g^+$ respectively. The insets in (a) and (b) show the Fourier transform of oscillating spectra ($3d\sigma_g$ ($v' = 0$) $\rightarrow$ $X^2\Sigma_g^+$ ($v'' = 0$)) and ($11d\sigma_g$ ($v' = 3$) $\rightarrow$ $X^2\Sigma_g^+$ ($v'' = 0$)) of both experiment (red) and theory (blue) respectively. (c) and (d) Fourier analysis of the observed and calculated TR-PES (Figure 1(b) and (d)) as a function of the photoelectron energy with a logarithmic scale colormap respectively. (e) and (f) Fourier phases of the experimental and simulated two-NIR-photon signal at 17.5 THz respectiverly.

the main-peaks in the two-NIR-photons region outside the cross-correlation time. This can be further quantified using the common frequency at 17.5 THz from the Fourier analysis in Fig. 2. The argument extracted from the complex amplitude of the FFT spectral components is defined as the phase, which defines the time at which a specific signal maximizes. The extracted phases are presented in Figure 2(e). The main-peak phases (green dots) are more or less constant about 1.5 rad, whereas the sub-peak phases (blue dots) have a decreasing trend (in absolute value) with increasing its kinetic energy. Overall, this leads to an increasing phase difference between the main and sub-peaks with kinetic energy. As such, the population of higher vibrational levels leads to a decrease of the relative time delay between the main and sub-peaks. Similarly, Figure 2(f) shows phases retrieved for the calculated spectrum. Interestingly, the calculations confirm the flat phases for the main-peaks and they also reproduce the large phase difference between the main- and sub-peaks at high kinetic energies. Therefore, the calculations correctly capture the different effects of the autoionizing resonances on the observation of the vibrational wave packet. Interestingly, the calculated sub-peaks phases stay flat as a function of kinetic energies, while the experimental data shows a decreasing trend (see Fig 2(e)). For the main-peaks, on the one hand, the relative contributions of the direct ionization pathways are less than those from the autoionization pathways, which is inferred from their relative energy distributions in Figure 1(a); on the other hand, the phase difference between the direct and the autoionization pathways are overall small (see Fig. S2 in Supplemental Material [48]), such that the observed phases do not vary much as a function of kinetic energy. For the sub-peaks, the direct and indirect pathway phase differences are large, and the direct ionization channel becomes dominant at low kinetic energies owing to the increase of photoionization cross sections towards the threshold, which result in a significant modulation on the observed phase with decreasing photoelectron energy (see the analytical estimation in the Supplemental Material [48]). Therefore, the main reason for the discrepancy between the experimental and simulated phases is attributed to the absence of direct photoionization pathways in the simulation.

The above-mentioned observations can be summarized into an intuitive mechanism behind the observation of wavepacket dynamics probed through the autoionizing resonances. The mechanism is depicted in Fig. 3 where the relevance PECs are shown. In the pump step, the XUV pulse centered around 14.15 eV creates a superposition of three vibronic states $b'\,^1\Sigma_u^+$ ($v' = 14, 15,$ and 16, solid red lines) through the vertical excitation from the ground state $X^1\Sigma_g^+(v' = 0)$.

During the cross-correlation time, the NIR-probe pulse launches the wavepacket from b' state to both $3d\sigma_g$ ($v' = 0$) and $11d\sigma_g$ ($v' = 3$) Rydberg states, since the wavepacket is still relatively well localized on the b' state in the FC region. In this situation, the vibrational wave packet formed from the three high-lying vibrational levels ($v' = 14, 15, 16$) in b' state and the $v' = 0$ in $3d\sigma_g$ state have large FC factors irrespective of the internuclear distance R. In contrast, the $v' = 3$ vibrational level in $11d\sigma_g$ Rydberg state has several nodes, meaning that the FC factors strongly depend on the internuclear distance R. In addition, the resonant transition between b' ($v' = 14$) and $11d\sigma_g$ ($v' = 3$) could be energetically suppressed as a consequence of their energy difference (~ 3.17 eV) is slightly larger than the total en-

ergy of two NIR photons (~ 3.11 eV). Considering these two aspects, the sub-peaks show a negligible contribution from the lowest b' ($v' = 14$) state. Since the two Rydberg states have much shorter lifetimes [20, 46] than the cross-correlation, the launched wavepacket instantaneously autoionize/decay to the N_2^+ $X^2\Sigma_g^+$ state. As a result, the main and sub-peaks appear at the same time in the spectrum.

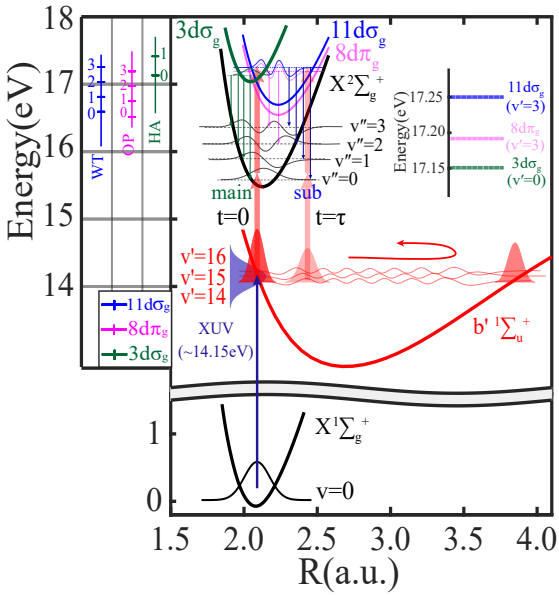

Figure 3: (Color online) Schematic PECs in the energy region of interest [33, 38]. The ground state of N_2 $X^1\Sigma_g^+$, ionic ground state N_2^+ $X^2\Sigma_g^+$, valence b' $^1\Sigma_u^+$ state, Rydberg state $11d\sigma_g$ and previously Ogawa progression $8d\pi_g$ both converging to A $^2\Pi_u$ N_2^+, and Rydberg state $3d\sigma_g$ converging to B $^2\Sigma_u^+$ N_2^+. HA: Hopfield absorption series [36, 37, 40]. OP: Ogawa progression[36, 37, 41]. WT: Worley third series [36, 47].

At time delays longer than the cross-correlation, an XUV-prepared wavepacket passes through the outer turning point of the b' state, see Fig. 3. During its passage back to the inner turning point, a transition between the b' state and the outer turning point of the $11d\sigma_g$ state occurs before a transition to the $3d\sigma_g$ state. This means that the sub-peaks generally reach their maxima earlier than the main-peaks in the time-resolved spectra beyond the cross-correlation time. Nevertheless, since the direct ionization pathway becomes dominant as the vibrational levels in the $X^2\Sigma_g^+$ ground state increase towards the ionization threshold, the interference between the two pathways leads to a significant modulation on the observed phases. Whereas, the indirect pathway is always dominant for the main-peaks, which results in the observed phases unaffected. The internuclear distance dependent FCs between the autoionizing states and the ionic state mainly affect the relative intensity of individual peaks, which could also essentially contribute to the interference term and varies the observed phases.

In summary, we have used TRPES to access the ultrafast wavepacket dynamics of N_2, probed through autoionizing Rydberg resonances with high temporal and spectral resolution. The observed photoelectron spectrum shows clear beating signals, and is well interpreted by a time-dependent quantum-mechanical calculation. Three dominant high-lying adjacent vibrational levels ($v' = 14, 15, 16$) in the b' valence state were prepared by the XUV pulse centered at 14.15 eV. Three autoionizing Rydberg states converging to the A $^2\Pi_u$ and B $^2\Sigma_u^+$ states of N_2^+ were then accessed by the NIR pulse and their signatures are identified in the spectrum, revealing interesting differences in both the phase and the amplitude of the observed b'-state wave-packet signals. This combined experimental and theoretical study demonstrates the important role of autoionizing resonances in TRPES of molecular wave packets and clarifies how these resonances affect the observables of TRPES. The insight gained from this work will support the design and interpretation of future experiments in this field.

This work was supported by ETH Zurich, the Swiss National Science Foundation through the NCCR-MUST and project no. 200021_172946. Work by A.T.L. was supported by the U.S. Department of Energy, Office of Science, Office of Basic Energy Sciences under Award Number DE-SC0023192.

† pengju.zhang@phys.chem.ethz.ch
‡ thu.le@uconn.edu

[1] A. H. Zewail, The Journal of Physical Chemistry A **104**, 5660 (2000).
[2] F. Krausz and M. Ivanov, Reviews of Modern Physics **81**, 163 (2009).
[3] F. Légaré, K. F. Lee, I. V. Litvinyuk, P. W. Dooley, A. D. Bandrauk, D. M. Villeneuve, and P. B. Corkum, Physical Review A **72**, 052717 (2005).
[4] A. S. Alnaser, B. Ulrich, X. M. Tong, I. V. Litvinyuk, C. M. Maharjan, P. Ranitovic, T. Osipov, R. Ali, S. Ghimire, Z. Chang, et al., Phys. Rev. A **72**, 030702 (2005).
[5] B. Feuerstein, T. Ergler, A. Rudenko, K. Zrost, C. D. Schröter, R. Moshammer, J. Ullrich, T. Niederhausen, and U. Thumm, Physical Review Letters **99**, 153002 (2007).
[6] F. Kelkensberg, C. Lefebvre, W. Siu, O. Ghafur, T. T. Nguyen-Dang, O. Atabek, A. Keller, V. Serov, P. Johnsson, M. Swoboda, et al., Physical Review Letters **103**, 123005 (2009).
[7] P. M. Kraus, A. Rupenyan, and H. J. Wörner, Phys. Rev. Lett. **109**, 233903 (2012).
[8] P. M. Kraus, D. Baykusheva, and H. J. Wörner, Phys. Rev. Lett. **113**, 023001 (2014).
[9] P. M. Kraus, B. Mignolet, D. Baykusheva, A. Rupenyan, L. Horný, E. F. Penka, G. Grassi, O. I. Tolstikhin, J. Schneider, F. Jensen, et al., Science **350**, 790 (2015), URL `http://www.sciencemag.org/content/350/6262/790.abstract`.
[10] Y. Nabekawa, Y. Furukawa, T. Okino, A. A. Eilanlou, E. J. Takahashi, K. Yamanouchi, and K. Midorikawa, Nature Communications **7**, 12835 (2016).
[11] D. R. Cyr and C. C. Hayden, The Journal of chemical physics **104**, 771 (1996).

[12] D. M. Neumark, Annu. Rev. Phys. Chem. **52**, 255 (2001), URL http://dx.doi.org/10.1146/annurev.physchem.52.1.255.

[13] T. Suzuki, L. Wang, and M. Tsubouchi, J. Phys. Chem. A **108**, 5764 (2004), ISSN 1089-5639, URL http://dx.doi.org/10.1021/jp0486043.

[14] G. Wu, P. Hockett, and A. Stolow, Physical Chemistry Chemical Physics **13**, 18447 (2011).

[15] A. von Conta, A. Tehlar, A. Schletter, Y. Arasaki, K. Takatsuka, and H. J. WÃ¶rner, Nature Communications **9**, 3162 (2018), ISSN 2041-1723, URL https://doi.org/10.1038/s41467-018-05292-4.

[16] M. Koch, T. J. A. Wolf, and M. Gühr, Phys. Rev. A **91**, 031403 (2015), URL https://link.aps.org/doi/10.1103/PhysRevA.91.031403.

[17] I. Wilkinson, A. E. Boguslavskiy, J. Mikosch, J. B. Bertrand, H. J. Wörner, D. M. Villeneuve, M. Spanner, S. Patchkovskii, and A. Stolow, The Journal of Chemical Physics **140**, 204301 (2014), https://doi.org/10.1063/1.4875035, URL https://doi.org/10.1063/1.4875035.

[18] V. Svoboda, N. B. Ram, R. Rajeev, and H. J. Wörner, The Journal of Chemical Physics **146**, 084301 (2017).

[19] E. R. Warrick, W. Cao, D. M. Neumark, and S. R. Leone, The Journal of Physical Chemistry A **120**, 3165 (2016).

[20] M. Eckstein, C.-H. Yang, F. Frassetto, L. Poletto, G. Sansone, M. J. Vrakking, and O. Kornilov, Physical Review Letters **116**, 163003 (2016).

[21] L. J. Zipp, A. Natan, and P. H. Bucksbaum, Physical Review A **95**, 061403(R) (2017).

[22] E. R. Warrick, J. E. BÃ¦khÃ¸j, W. Cao, A. P. Fidler, F. Jensen, L. B. Madsen, S. R. Leone, and D. M. Neumark, Chemical Physics Letters **683**, 408 (2017).

[23] C. Marceau, V. Makhija, P. Peng, M. Hervé, P. B. Corkum, A. Y. Naumov, A. Stolow, and D. M. Villeneuve, Physical Review A **99**, 023426 (2019).

[24] M. Fushitani, Y. Toida, F. Légaré, and A. Hishikawa, Optics Express **27**, 19702 (2019).

[25] M. Fushitani, S. T. Pratt, D. You, S. Saito, Y. Luo, K. Ueda, H. Fujise, A. Hishikawa, H. Ibrahim, F. Légaré, et al., The Journal of Chemical Physics **154**, 144305 (2021).

[26] A. von Conta, M. Huppert, and H. J. Wörner, Rev. Sci. Instrum. **87**, 073102 (2016).

[27] V. Véniard, R. TaÃ¯eb, and A. Maquet, Physical Review Letters **74**, 4161 (1995).

[28] S. Xue, H. Du, B. Hu, C. D. Lin, and A.-T. Le, Phys. Rev. A **97**, 043409 (2018).

[29] M. Seel and W. Domcke, The Journal of Chemical Physics **95**, 7806 (1991).

[30] R. de Vivie-Riedle, K. Kobe, J. Manz, W. Meyer, B. Reischl, S. Rutz, E. Schreiber, and L. Wöste, The Journal of Physical Chemistry **100**, 7789 (1996).

[31] Y. Arasaki, K. Takatsuka, K. Wang, and V. McKoy, The Journal of Chemical Physics **112**, 8871 (2000).

[32] D. Stahel, M. Leoni, and K. Dressler, The Journal of Chemical Physics **79**, 2541 (1983).

[33] D. Spelsberg and W. Meyer, The Journal of Chemical Physics **115**, 6438 (2001).

[34] J. S. Ajay, K. G. Komarova, F. Remacle, and R. D. Levine, Proceedings of the National Academy of Sciences **115**, 5890 (2018).

[35] P. Cremaschi, A. Chattopadhyay, P. Madhavan, and J. Whitten, Chemical Physics **109**, 117 (1986).

[36] W. M. Kosman and S. Wallace, The Journal of Chemical Physics **82**, 1385 (1985).

[37] L.-E. Berg, P. Erman, E. KÃ¤llne, S. Sorensen, and G. Sundström, Physica Scripta **44**, 131 (1991).

[38] D. A. Little and J. Tennyson, Journal of Physics B: Atomic, Molecular and Optical Physics **46**, 145102 (2013).

[39] W. C. Ermler, J. P. Clark, and R. S. Mulliken, The Journal of Chemical Physics **86**, 370 (1987).

[40] M. Raoult, H. L. Rouzo, G. Raseev, and H. Lefebvre-Brion, J. Phys. B: At. Mol. Phys. **16**, 4601 (1983).

[41] M. Ogawa, Can. J. Phys. **42**, 1087 (1964).

[42] P. Peng, C. Marceau, M. Hervé, P. B. Corkum, A. Y. Naumov, and D. M. Villeneuve, Nature Communications **10**, 5269 (2019).

[43] R. Robinett, Physics Reports **392**, 1 (2004).

[44] P. Cörlin, A. Fischer, M. Schönwald, A. Sperl, T. Mizuno, U. Thumm, T. Pfeifer, and R. Moshammer, Physical Review A **91**, 043415 (2015).

[45] H. Lefebvre-Brion and C. M. Moser, The Journal of Chemical Physics **43**, 1394 (1965).

[46] M. Reduzzi, W.-C. Chu, C. Feng, A. Dubrouil, J. Hummert, F. Calegari, F. Frassetto, L. Poletto, O. Kornilov, M. Nisoli, et al., Journal of Physics B: Atomic, Molecular and Optical Physics **49**, 065102 (2016).

[47] J. B. Randazzo, P. Croteau, O. Kostko, M. Ahmed, and K. A. Boering, The Journal of Chemical Physics **140**, 194303 (2014).

[48] See Supplemental Material at [URL will be inserted by publisher] for a detailed account of the relative time differences between main- and sub-peaks, the phases of the direct pathways and an analytical model for the interference between direct and indirect pathways.